Intrinsic photophysics of nitrophenolate ions studied by cryogenic ion spectroscopy

Journal:	*Physical Chemistry Chemical Physics*
Manuscript ID	CP-ART-09-2018-006078.R1
Article Type:	Paper
Date Submitted by the Author:	24-Oct-2018
Complete List of Authors:	Dodson, Leah; University of Colorado Boulder, JILA and NIST Zagorec-Marks, Wyatt; University of Colorado Boulder, JILA and Department of Chemistry Xu, Shuang; University of Colorado at Boulder, JILA and Department of Physics Smith, James; University of Colorado at Boulder, JILA and Department of Chemistry WEBER, J. Mathias; University of Colorado, JILA and Department of Chemistry

Intrinsic photophysics of nitrophenolate ions studied by cryogenic ion spectroscopy*

Leah G. Dodson,[1,†] Wyatt Zagorec-Marks,[2,†] Shuang Xu,[3] James E. T. Smith,[2] and J. Mathias Weber[2,‡]

[1]*JILA and NIST, University of Colorado, 0440 UCB, Boulder, CO 80309-0440, USA*

[2]*JILA and Department of Chemistry, University of Colorado, 0440 UCB, Boulder, CO 80309-0440, USA*

[3]*JILA and Department of Physics, University of Colorado, 0440 UCB, Boulder, CO 80309-0440, USA*

Abstract

The intrinsic photophysics of nitrophenolate isomers (*meta*, *para*, and *ortho*) were studied at low temperature using photodissociation mass spectrometry in a cryogenic ion trap instrument. Each isomer has distinct photophysics that affect the excited state lifetimes, as observed experimentally in their spectroscopic linewidths. Visible-light-induced excitation of *m*-nitrophenolate gives rise to well-resolved vibronic features in the spectrum of the S_1 state. The *para* and *ortho* isomers have broad spectra – even at cryogenic temperatures – due to their shorter exited state lifetimes and spectral congestion. We present computational evidence for mixing of the first and second excited states of *o*-nitrophenolate, leading to significant additional broadening in the experimental spectrum.

---

* Electronic supplementary information (ESI) available.

† L. G. Dodson and W. Zagorec-Marks contributed equally to this work.

‡ Corresponding author; email: weberjm@jila.colorado.edu.

Introduction

Charge transfer chromophores are an important class of molecular systems[1] with applications ranging from solar energy conversion[2-4] to optical materials,[5, 6] and they occur in many biochromophores.[7] Nitrophenolates (NPs, see Fig. 1) are interesting, prototypical molecules for the study of charge transfer chromophores. In these systems, the three isomers constituting a set of simple chromophores,[8] electronic excitation initiates electron transfer from the negatively charged phenolate moiety to the nitro group. NPs are attractive targets for study, since they are sufficiently small to make quantum chemical calculations seem feasible, while at the same time allowing investigations of substitution effects on their electronic spectra and dynamics. Consequently, there has been much interest in the photophysics and photochemistry of NPs.[9-18]

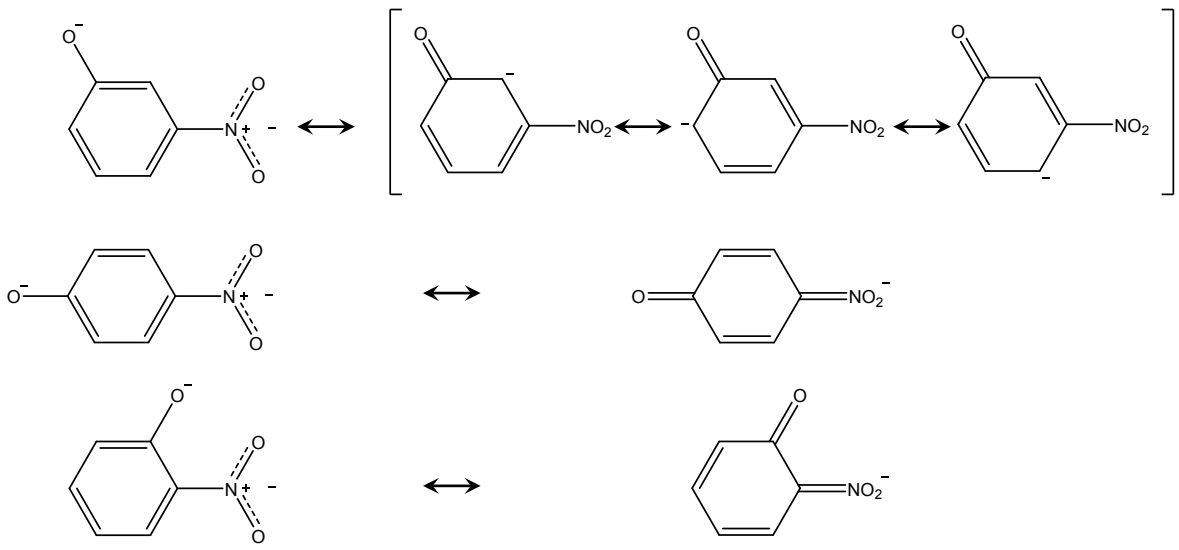

Fig. 1 Resonance structures of *meta* (top), *para* (middle), and *ortho* (bottom) isomers of nitrophenolate, adapted from Wanko *et al*.[11]

The most immediate effect of substitution positions in NPs can be observed by measuring and comparing the UV/vis absorption spectra of *m*-, *p*-, and *o*-NP. All isomers absorb in the visible

spectral range, but the absorption peak energies vary significantly. Substitution at different positions does not only affect excited state energies, it also has a pronounced effect on excited state dynamics. A recent study by Michenfelder *et al*.[18] showed that *o*- and *p*-NP generally have much shorter excited state lifetimes (≤ 300 fs) than *m*-NP (up to ca. 5 ps). The solvent environment has a strong influence on the excited state dynamics, too, as S_1 lifetimes are generally much shorter in aqueous solution than in organic solvents.[18]

Consideration of only solution data leads to a complicated picture that defies an intuitive understanding of the photophysics of these systems, due to strong solvation effects. In addition, while several quantum chemical descriptions of NP excited states have been published, solution data only allow a relatively crude comparison with computational results, since the spectra are broad, and the treatment of the chemical environment is either quite expensive (for explicit solvent molecules) or necessitates approximations whose quality is not easy to predict (for continuum models).

A particularly interesting experimental avenue that aims to recover the intrinsic photophysics of molecular ions is the spectroscopy of mass-selected species, as well as their complexes with solvent molecules. Brøndsted Nielsen and coworkers have investigated NPs extensively over the last decade.[9-15] Their results on the absorption spectra of NP ions *in vacuo* show that the apparent vertical excitation energies of the S_1 state of *p*- and *o*-NP are quite similar (at ca. 23000 cm^{-1} and 22100 cm^{-1}, respectively), while that of *m*-NP is found significantly further to the red (18800 cm^{-1}). This difference can be intuitively understood through charge distribution and resonance stabilization arguments.[11] The difference in the electronic structure also allows a zero-order explanation of the difference in excited state lifetimes,[18] since the charge distribution

results in a much stronger charge transfer character of the S_1 state for *m*-NP than for *ortho* and *para* isomers, which have more of a $\pi \rightarrow \pi^*$ character.

While the current literature allows a rough understanding of the photophysics of NPs, the absorption spectra observed at room temperature are very broad, even those reported *in vacuo*.[11] This leaves important questions about the excited state vibrational structure, and – as a benchmark for a computational description of these systems – about their S_1 electronic band origins. In particular, the role of low-frequency vibrational modes in excited state geometries, which are important for the understanding of excited state dynamics,[18] is not understood. As mentioned above, experiments *in vacuo* are highly valuable in eliminating solvent effects, but at room temperature they still suffer from hot bands, which obscure band origins and result in significant spectral congestion. Preparation of cold target ions leads to the suppression of hot bands, and allows much more detailed insight into the excited state properties.

In the current work, we present electronic photodissociation spectroscopy of mass selected *m*-, *p*-, and *o*-NP ions *in vacuo*, prepared in a cryogenic ion trap. Our experimental results show that the spectra of *o*- and *p*-NP remain broad, even at cryogenic temperatures. In contrast, the spectrum of *m*-NP exhibits sharp vibrational features that allow detailed insight into the vibrational structure on the excited state surface. We interpret our results in the framework of time-dependent density functional theory.

Methods

Experimental

Solutions of *o*- and *p*-NP were prepared by dissolving nitrophenolate sodium salts (97% ArkPharm, 95+% Matrix Scientific) in methanol (ACS, VWR International) to give a NP anion

concentration of of 1 mM. Solutions of *m*-NP were prepared by dissolving *m*-nitrophenol (98+%, Alpha Aesar) in methanol with a concentration of 1 mM followed by the addition of a few drops of 50 mM aqueous KOH solution. All solutions formed were yellow/orange and were used in electrospray ionization without further purification. The apparatus used in this experiment has been described in detail elsewhere.[19] Briefly, the NP solutions were sprayed out of a needle capillary with inner diameter 75 μm at a flow rate of 50 μL/hour. The spray employed N_2 as sheath gas, and entered a heated capillary with inner diameter 760 μm at the entrance of a sequence of differential pumping stages. After exiting the capillary, the ions passed through a skimmer and into a series of octopole ion guides. In the first octopole ion guide, ion packets were formed using pulsed end cap electrodes. Upon reaching the final differential pumping stage, these packets were injected into a 3D quadrupole ion trap, which was cooled by a closed-cycle helium cryostat to cryogenic temperatures, (30 ± 5) K in the present work. Helium gas was pulsed into the trap and used as a buffer gas to provide collisional cooling. Ion packets were held in the trap for 95 ms to allow sufficient cooling time, after which they were mass separated in a Wiley-McLaren time-of-flight (TOF) mass spectrometer. We note that attempts at messenger tagging the ions under study with N_2 or D_2 were unsuccessful.

Upon injection into the TOF, ions of interest were mass selected by a pulsed mass gate and then irradiated by the output of a pulsed (5–7 ns) BBO-based optical parametric converter system (OPC) pumped by the third harmonic of a Nd:YAG laser (355 nm), producing radiation in the wavelength range from 357–710 nm (bandwidth 5 cm^{-1}). The spectra reported in this work were acquired employing several different crystal settings of the OPC for different regions of the signal radiation, as well as sum-frequency mixing of the signal wave with the fundamental of the Nd:YAG pump laser. Some exploratory measurements on *p*-NP were performed using a Nd:YAG-

pumped dye laser (Coumarin 440, 0.1 cm^{-1} laser linewidth, see Results and Discussion). Fragmentation upon photon absorption was monitored by secondary mass analysis using a reflectron, detecting the fragment ions on a dual microchannel plate detector. Brøndsted Nielsen and coworkers[9-14] found the two dominant photofragment channels to be the formation of NO_2^- and the loss of NO, and that sequential, incoherent absorption of two photons was needed for fragment formation. Throughout this work, we monitored the loss of NO to record the photofragmentation spectra. The laser pulse energy was measured using a pyroelectric joulemeter.

The mass spectrometer and ion trap were run at a repetition rate of 10 Hz, and the light source was pulsed at 5 Hz repetition rate, allowing for the collection of a signal with and without laser irradiation. The subtraction of these two allowed subtraction of the background signal resulting from collision-induced fragmentation from the laser-induced signal. The resulting difference signal was corrected for photon fluence, assuming two-photon absorption.

Computational

The literature record shows a number of approaches that have previously been used to describe the spectra of NPs. In some studies, MP2 calculations were undertaken to describe the geometry of the NP ground state, with vertical excited state energies calculated from the optimized ground state geometry.[9-11] Excited state energies have been calculated using coupled-cluster CC2 and time-dependent density functional theory (TD-DFT), with generally good agreement found between vertical energies calculated using CC2 and experimental results.[13] Diagnostics implemented in CC2 calculations reveal that nitrophenolate anions have multi-reference character, making any single-reference method problematic. However, the validity of using CC2 calculations

to describe nitrophenolate ions was established through comparison with SORCI vertical excitation energies.[11]

In this work, we require not only the vertical excitation energies used in past studies to evaluate our experimental results, but we also need excited state optimized geometries and harmonic vibrational frequencies (of both the ground and excited state structures). This information is necessary to both assign vibronic transitions in the experimental spectra, and interpret the broadening mechanisms. As mentioned above, the multi-reference character of nitrophenolates means that single-reference methods are not very reliable for the description of these systems. However, the computational cost of using multi-reference methods for excited state geometry calculations and vibrational spectra would be prohibitive. For these reasons, we turn to density functional theory (DFT) methods, to take advantage of computationally feasible excited state properties available through TD-DFT. We elected to use a range-separated hybrid functional (CAM-B3LYP[20]) because, as noted by Wanko *et al*.,[11] the charge transfer nature of the NP excited states introduces problems for standard DFT functionals. Kozłowska *et al*. evaluated the performance of a wide variety of general and hybrid functionals, including CAM-B3LYP, finding that the generalized gradient approximation functions perform better than range-corrected functionals at reproducing the vertical electronic excitation energy for *p*-NP.[16] However, we chose to use the CAM-B3LYP method, rather than using a functional that was not range-corrected, because other functionals (e.g. B3LYP) resulted in a lowering of the energy of dark charge transfer states. This resulted in incorrect ordering of excited states in TD B3LYP calculations, which is inconsistent with the ordering found in time-dependent Hartree Fock (TD HF), as is often seen for transitions with significant charge-transfer character.[21, 22] The CAM-B3LYP functional was recently utilized by Panja, *et al*. to evaluate the UV/vis absorption spectra of multiply-substituted

nitrophenolates, and generally found to yield better agreement between experimental spectra and values obtained using CAM-B3LYP, than for the simpler hybrid functional B3LYP,[17] and the TD CAM-B3LYP results gave excited state ordering that are consistent with TD HF calculations.

We performed ground and excited state geometry optimizations using the CAM-B3LYP functional and the aug-cc-pVDZ basis. Exploratory calculation were carried out with a larger basis (aug-cc-pVTZ basis), but the vertical excitation energies changed less than 2% when increasing to a triple-zeta basis so the double-zeta basis was considered to be sufficient for comparison with the experimental results. Three-dimensional potential energy surfaces for the ground and excited states were obtained through relaxed geometry scans over the torsion angle about the C-N bond, and the angle defining the pyramidalization of the NO_2 group. Minimum energy structures were identified using harmonic frequency analysis. Molecular orbitals were generated using the same method. To assign the vibrationally-resolved experimental electronic spectrum of *m*-NP, the temperature-dependent Franck-Condon spectrum was simulated based on the optimized ground and excited state geometries, utilizing Duschinsky rotations. A Natural Bond Orbital analysis was carried out using NBO 3.1.[23] These calculations operate at the CAM-B3LYP level with the same basis referenced above. Natural populations were extracted from these calculations, and electron density difference plots were generated using GaussView. All calculations were carried out using Gaussian 16.[24]

Results and Discussion

Overview

Fig. 2 shows the photodissociation spectra of the S_1 electronic bands of all three isomers of NP, acquired at a trap temperature of (30 ± 5) K. The spectrum of *m*-NP shows an extended

progression of well-resolved vibrational levels, with the first sharp features beginning at ca. 16000 cm^{-1}, and the band envelope centered around 17300 cm^{-1}. In contrast, the S_1 band of *p*-NP peaks at 22960 cm^{-1}, with an onset at around 22450 cm^{-1}, but the overall band is broad, and there are no resolved vibrational structures. The *o*-NP spectrum shows a complicated sequence of broad bands, centered around 23000 cm^{-1}, with an onset around 20500 cm^{-1}, also without any resolved vibrational features. As discussed by Brøndsted Nielsen and coworkers,[11] the difference in peak absorption energies can be qualitatively explained with resonance stabilization arguments depicted in Fig. 1. In their ground states, *o*- and *p*-NP can be described as resonances between an aromatic and a quinoid structure, the latter carrying a formal negative charge on the nitro group, forming double bonds of both substituents with the ring. This resonance stabilizes the ground state in both cases. In *m*-NP, the quinoid structure cannot be realized, and the absence of this mechanism for ground state stabilization reduces the energy difference between S_0 and S_1. In the following sections, we will discuss the spectra of each isomer in detail.

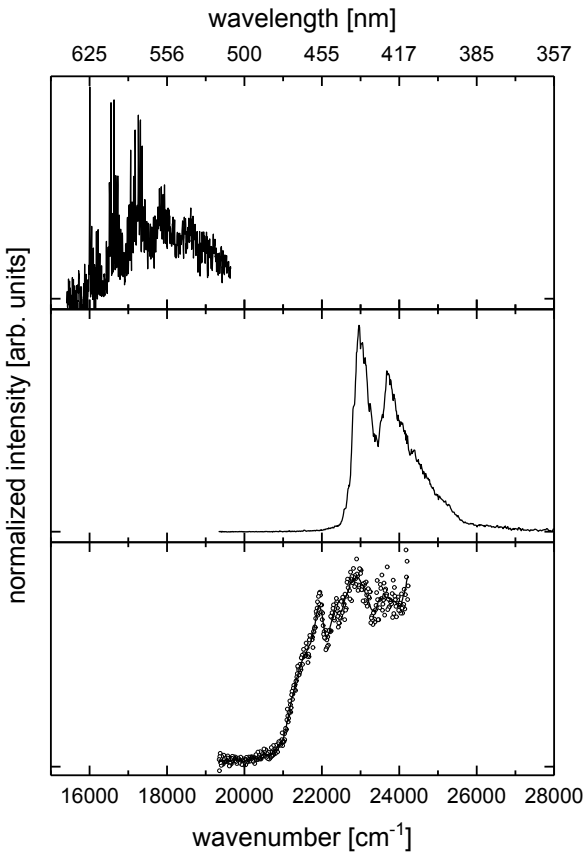

Fig. 2 Overview of the spectra of *m*- (top), *p*- (center), and *o*-NP (bottom) in their respective S_1 regions at (30 ± 5) K trap temperature. For *m*- and *p*-NP, the full lines connect the data points; for *o*-NP, the data points are shown as open circles, while the full line represents a 15-point gliding average.

Meta-Nitrophenolate

Of the three NP isomers, *m*-NP has the weakest calculated oscillator strength (see Table 1) in the $S_0 \rightarrow S_1$ transition, consistent with a strong charge transfer character. The charge transfer character of *m*-NP can be seen quite clearly in the electron density difference plot (Fig. 3) as electron density moves from the phenolate oxygen atom (loss of electron density upon excitation shown in yellow) to the nitro group (gain in electron density upon excitation shown in purple).

This assignment is also consistent with the small overlap between the two main orbitals involved in the transition (see Fig. S3 in ESI). The change in the dipole moment upon electronic excitation is 7.5 Debye, again consistent with a charge transfer event. The spectrum of *m*-NP (see Fig. 2 and 4) shows well-resolved vibrational bands. The first sharp peak is found at 16003 cm^{-1}, and we assign it to the transition between the vibrational ground states of the ground and excited electronic states, i.e., the band origin, (0_0^0). In the remainder of this work, we denote transitions with $Q_{v"}^{v'}$, where Q denotes the label of the vibrational mode, and *v*" and *v*' are the numbers of quanta in mode Q in the lower and upper electronic state, respectively. The vibrational modes are numbered in order of increasing vibrational frequency in the S_1 state. The vibrational bands seen in this spectrum show a regular spacing of ca. 45 cm^{-1} close to the origin. Towards higher energies, there are several regions with high intensity, spaced by 620–640 cm^{-1}, and although the bands are sharp, the photodissociation signal does not return to baseline, signaling increased spectral congestion. Within these regions of high intensity, individual bands are again separated by 35–45 cm^{-1}. The overall envelope of this spectrum is consistent with the room temperature data reported by Brøndsted Nielsen and coworkers (see Fig. S4).[11]

Table 1 Experimental and calculated overview data (vertical excitation energies, band origins, oscillator strengths). Transitions are given in cm^{-1}. Calculations were performed using CAM-B3LYP/aug-cc-pVDZ.

	m-NP	*p*-NP	*o*-NP
Experimental onset[a]	16003	22450	20500
Experimental vertical transition	17300	22960	23000
Calculated S_1 properties			
Band origin energy[b]	15849	18497	17604
Vertical transition energy	18761	28772	27130
Oscillator strength	0.0268	0.5048	0.2033
Orbitals (contribution)	HOMO → LUMO	HOMO → LUMO	HOMO → LUMO+2
Calculated S_2 properties			
Band origin energy[b]	N/A [c]	N/A [c]	21700
Vertical S_2 (calc.)	27540	30980	26963
S_2 oscillator strength (calc.)	0.0000	0.0000	0.0001

[a] For *m*-NP, this entry is the energy of the 0_0^0 band; for *p*- and *o*-NP, the onset of the spectrum is listed.

[b] Values have been corrected for zero-point energies.

[c] Band origin energies for *m*- and *p*-NP were not calculated in the present work for S_2.

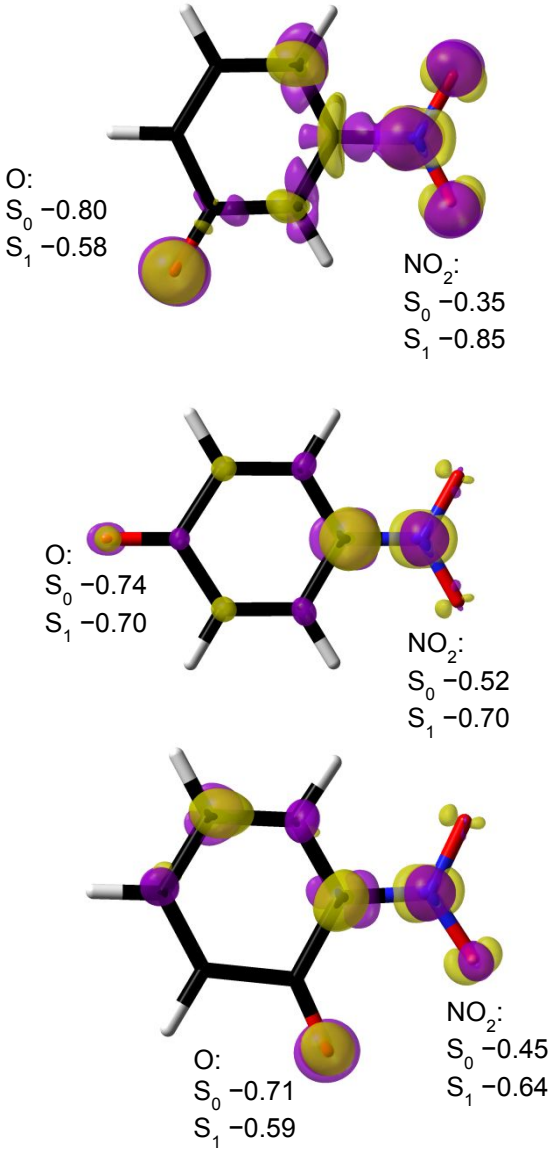

Fig. 3 Electron density difference plots for *meta* (top), *para* (center), and *ortho* (bottom) isomers of nitrophenolate. Purple regions indicate an increase of electron density upon electronic transition, while yellow regions indicate a decrease of electron density upon electronic transition. The density difference for *o*-nitrophenolate was calculated for the S_1 state. Listed are the charges on the NO_2 and O groups for each isomer in the S_0 and S_1 states. Charges calculated using a Natural Population Analysis, given in e.

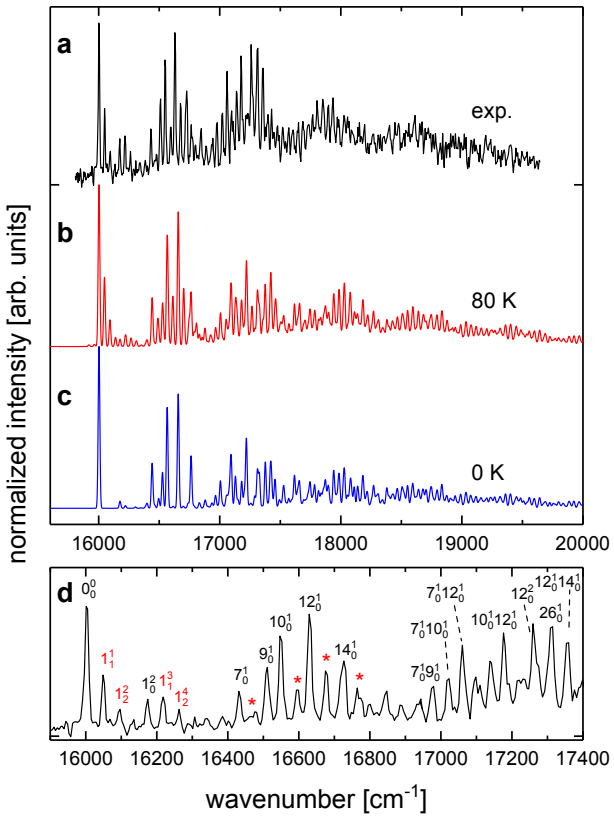

Fig. 4 Top panel: experimental spectrum of *m*-NP (a), compared to Franck-Condon simulations at 80 K (b) and 0 K (c). Bottom panel: Zoom of the first 2400 cm^{-1} above the origin, with assignments of selected peaks (d); hot bands are marked in red, red asterisks label peaks whose main contribution comes from a hot band with one quantum in the nitro torsion vibration.

We use the results of our CAM-B3LYP calculations in order to interpret the spectrum in detail. The *meta* isomer is calculated to have a planar excited state, and the transition can be characterized as a pure HOMO → LUMO transition.[11] The structures of *m*-NP in its ground and first excited singlet states are shown in Fig. 5. Both are planar, with C_S symmetry (see Fig. S5 for the ground and first excited potential energy surfaces). The transition between S_0 and S_1 can therefore be described as X(^{1}A') → A(^{1}A') in spectroscopic notation. The calculated vertical

transition energy is 18761 cm^{-1}, which is higher than the center of gravity of the experimental band, but within the observed band. The calculated 0_0^0 band, is at 15849 cm^{-1}. This value is rather close to the experimental value, but the agreement is likely to be fortuitous. The oscillator strength of the vertical transition is 0.0268, which is the lowest value of the three isomers, in keeping with the expected behavior.

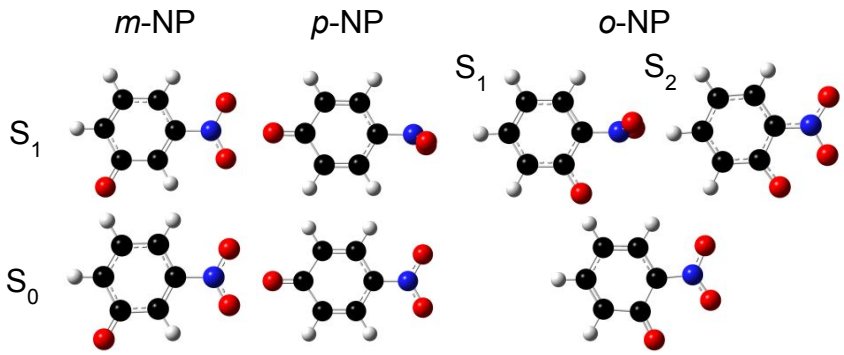

Fig. 5 Optimized geometries for *m*-, *p*-, and *o*-NP, in their ground and first excited states, calculated using CAM-B3LYP. Excited state geometries were optimized for the S_1 state, for *meta* and *para* isomers, and for the S_1 and S_2 states for the *ortho* isomer.

The main geometry change upon excitation is a 3% decrease in the C-N bond length and a 4% increase in the N-O bond length, suggesting that one can expect the signatures of Franck-Condon active vibrational modes involving these coordinates. However, typical values for C-N or N-O stretching modes are greater than 1000 cm^{-1}, while the spacing of the vibrational features of ca. 45 cm^{-1} suggests that a vibrational mode with much lower frequency is responsible for the high apparent density of vibrational levels.

Fig. 4 shows two Franck-Condon simulations based on harmonic wave functions in comparison with the experimental spectrum, one at zero K, and one at 80 K. Overall, the simulation

at 80 K qualitatively recovers the experimental spectrum quite well. Interestingly, the simulation temperature is significantly higher than the trap temperature in the experiment (30 K). Before we discuss the ion temperature further, we will first use the simulations to assign the observed vibrational bands.

The simulation at 80 K produces hot bands in the nitro torsion vibration, ω_1, i.e., the torsion around the C-N bond. This is the lowest frequency mode in both the ground and excited electronic states, with harmonic approximation values at 41 cm^{-1} and 77 cm^{-1} respectively, see Table S1 in the ESI. The torsion is rather anharmonic (see Fig. S6 in ESI). In the S_0 state, it can be described as a hindered rotor with a 1890 cm^{-1} barrier at 90°, while the S_1 state shows a local minimum at 90°, 1400 cm^{-1} higher than the planar configuration, and 1600 cm^{-1} barriers at ca. ±60° separating the planar and twisted configurations. In order to optimize the agreement between simulation and experiment the torsion frequency in the S_1 state was set to 87 cm^{-1}. Every transition belonging to a principal Franck-Condon active mode is accompanied by hot bands on the high energy side, originating from thermally populated vibrational levels in S_0 with one or two quanta in the nitro torsion mode, and these hot bands are the source of the high density of vibrational features in the spectrum. Tables of vibrational modes and assigned peaks are given in the ESI.

The simulation at zero K shows the principal Franck-Condon active modes, removing the hot bands, and allowing easier spectral assignment. In this simulation, the first band with significant intensity is due to the overtone of the nitro torsion, i.e., the 1_0^2 band (transitions with odd Δv_1 are symmetry-forbidden), which coincides with the onset of a series of features at 16175 cm^{-1}. Like all features in this spectrum, this band carries a sequence of hot bands (here: 1_1^3, 1_2^4, and 1_3^5, see Table S2 in the ESI).

After the band origin and the signature of the nitro torsion overtone, there is a cluster of intense peaks between 16390 cm^{-1} and 16910 cm^{-1}. We assign the first peak in this band at 16434 cm^{-1} to 7_0^1, where ω_7 can be characterized as an in-plane phenolate bending motion coupled to the in-plane nitro wagging motion and a ring deformation. In the same cluster of peaks, we find the transitions 9_0^1 (in-plane phenolate bending/ring deformation), 10_0^1 (ring deformation), 12_0^1, and 14_0^1 (both of the latter are ring deformation/nitro scissoring modes). We will refer to the modes forming this group of transition as group 1 modes; they are listed in Table S3 in the ESI.

The next region with high intensity (16900–17590 cm^{-1}) contains second order combination bands of ω_7, ω_9, ω_{10}, ω_{12}, and ω_{14}, as well as the overtones of ω_{10} and ω_{12} (with $\Delta v = 2$). Other overtones are also assignable, but are weaker (see Table S4 in the ESI). In addition, ($v'' = 0 \rightarrow v' = 1$) transitions involving modes based on C-N stretching/NO_2 stretching motions (ω_{26}, ω_{28}, ω_{31}, denoted as group 2 modes) appear prominently in this region of the spectrum. The third region with high intensity is based on second order combination bands of group 1 modes with group 2 modes, as well as third order combination bands of group 1 modes, see Table S5 in the ESI. At higher energies (ca 2200 cm^{-1} above the band origin), the spectrum becomes too congested to assign. This is not surprising, since excitation in this region will end in vibrational levels that are significantly above the calculated barrier in the torsional potential energy curve (ca. 1600 cm^{-1}), and the corresponding density of vibrational states, together with likely coupling effects between the many vibrational modes will result in strong spectral congestion, even for the Franck-Condon simulation at 0 K.

As mentioned above, while the trap temperature in our experiments was 30 K, the best agreement between simulation and experiment is reached for a simulation temperature of 80 K. The relative intensities of the 0_0^0 band and its hot bands were used as the relevant figure of merit,

since the spectrum is relatively clean in this region. This ratio should therefore be least sensitive to complications arising from the interaction of several vibrational modes, and the hot bands from the lowest frequency mode will be most sensitive to ion temperature. A more detailed temperature determination using measurements at different temperatures (see the ESI) yields an ion temperature of (65 ± 5) K as the best estimate. The observed discrepancy between trap temperature and simulation temperature is due to both experimental and computational issues. Radio frequency ion traps are known[25-27] to lead to heating by driving collisions between the buffer gas and the trapped ions. In addition, the presence of residual gas in the trap during ion extraction can also lead to some heating. Neither of these effects can be easily quantified experimentally in the present experiment, since deviation from optimal trapping and extraction parameters leads to severe losses in the parent ion intensity, which – together with the low absorption cross section and the need for absorption of two photons – precludes the measurement of the spectrum with a series of other experimental parameters. There is also an uncertainty in the computations. For example, Franck-Condon simulations using the B3LYP functional yield the best fit between simulation and experiment for a simulation temperature of 150 K, whereas CAM-B3LYP yields 80 K. Moreover, the hot bands allowing the temperature estimate in the simulations are based on transitions involving the very anharmonic nitro torsion mode. It is easy to see that the simulation is not accurate in the quantitative representation of this mode, as the sequence of bands based on Δv = +2 is strongly underestimated by the simulation (see Fig. 4). We assume that the ion temperature is in the range of 60–80 K. This estimate is in line with earlier experiments at similar trap temperatures, where we were able to form weakly bound complexes of a large molecular dication with N_2 molecules, and were able to estimate the ion temperature based on the calculated binding energy of the N_2 adducts.[28]

The linewidth in the experimental spectrum allows a rough estimate of a lower limit of the excited state lifetime. The first ten well-resolved lines in the spectrum have an average line width at half-maximum of (10.4 ± 1.2) cm^{-1}. Using the rotational constants obtained through our electronic structure calculations, a simulation of the rotational envelope at 80 K using the PGOPHER program[29] suggests that the envelope of the rotational band contour (individual rotational lines cannot be resolved) should have a width of ca. 8 cm^{-1}. A convolution with the bandwidth of the light source (ca. 5 cm^{-1}) leads to an expected final linewidth of 9.4 cm^{-1}. With lifetime broadening as an obvious candidate for the observed linewidth, a lifetime of ca. 1.2 ps would be compatible with the observed linewidth of 10.4 cm^{-1}. This value is in the range of lifetimes observed for *m*-NP in recent ultrafast experiments (0.5–5.6 ps),[18] even though our estimate is admittedly rather crude. We note, however, that the shorter lifetimes reported by Michenfelder *et al*. were measured in polar solvents, while nonpolar solvents yielded lifetimes around 5 ps. We would expect the absence of solvent molecules, as in our experiment, to be more compatible with a nonpolar solvent environment, unless the solvent molecule would help increase the excited state lifetime. Treating the estimate of 1.2 ps as a lower limit for the S_1 lifetime is therefore in rough agreement with the ultrafast experiments reported by Michenfelder *et al*.

Para-Nitrophenolate

In contrast to the spectrum of *m*-NP, the spectrum of *p*-NP is broad, even at low temperatures (see Fig. 6). The spectrum has a smooth onset at ca. 22450 cm^{-1}, and shows peaks at 22960 cm^{-1} (which we take to be the vertical excitation energy) and 23690 cm^{-1}. There is some partially resolved substructure throughout the first peak, with shoulders spaced by 100–130 cm^{-1}, but no well-resolved features are observed. Exploratory measurements on the low energy side of

the first main peak with ca. 2 cm^{-1} step size (using a dye laser, see Methods) confirm this observation, as they showed the same shoulders, but no other resolved features.

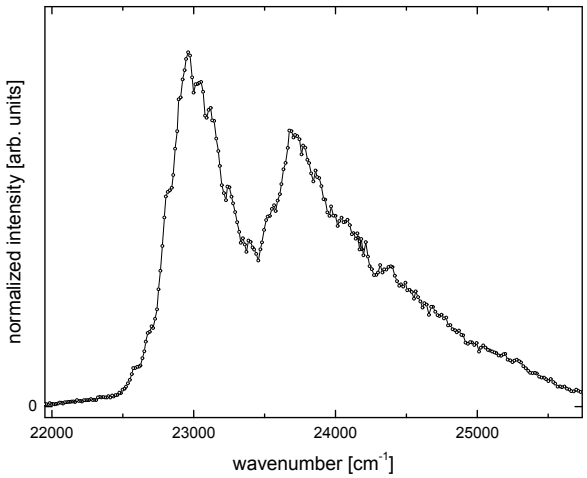

Fig. 6 Spectrum of *p*-NP.

Excited state calculations yield a vertical excitation energy at 28772 cm^{-1}, substantially overestimating the experimentally determined value, and its oscillator strength is predicted to be the strongest of the three isomers (f = 0.5048). The band origin is calculated to be at 18497 cm^{-1} above the ground state. The calculations reveal large geometry differences between the ground and excited states, particularly for the nitro group. While the molecule is planar in the ground state (C_{2v} symmetry), the nitro group is twisted around the C-N bond (90°) and slightly pyramidalized on the N atom (out-of-plane angle ca. 30°, see Figs. 5 and 7) in the first excited state. In the Franck-Condon region, there is a saddle point with planar structure, but this geometry is calculated ca. 9300 cm^{-1} above the relaxed S_1 geometry. As a result, excitation in the Franck-Condon region will launch vibrational motion along the nitro torsion and pyramidalization coordinates. The *p*-NP isomer exhibits less-pronounced charge transfer upon electronic excitation, compared to *m*-NP, as can be seen visually in the electron density difference plots (Fig. 3), with a change in the dipole

moment of 2.4 Debye. From the orbital plots, we characterize the vertical transition as more closely resembling a $\pi \rightarrow \pi^*$ transition (see Fig. S3).

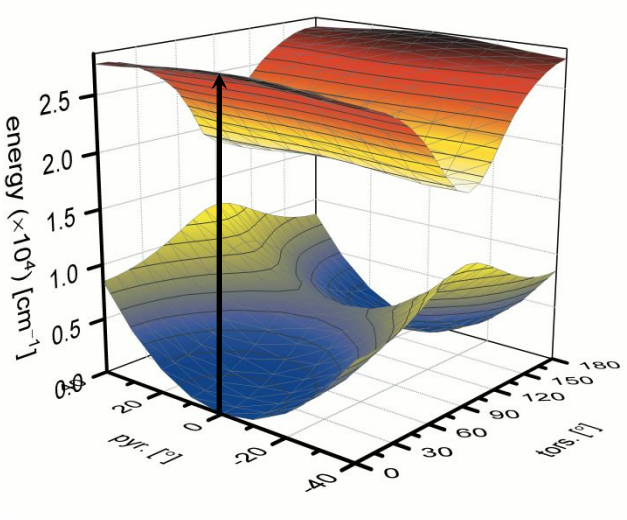

Fig. 7 Potential energy surfaces for the S_0 and S_1 states of *p*-NP. The surface was obtained at CAM-B3LYP/aug-cc-pVDZ with a relaxed scan over the nitro torsion (tors.) and pyramidalization (pyr.) coordinates. The black arrow indicates the vertical excitation from the relaxed ground state. Energies are given relative to the ground state minimum, in cm^{-1}.

The lack of sharp vibrational structure in the spectrum is a consequence of two effects. One is the large geometry difference between S_0 and S_1 for *p*-NP. Recalling the spectrum of *m*-NP, one would expect strong spectral congestion for an excitation so high above the electronic band origin, given the presence of low frequency vibrations, which will complicate the spectrum even at 0 K. The vibration that one would expect to be the main cause of this congestion is the low lying nitro torsion (calculated to be 96 cm^{-1} and 257 cm^{-1} in S_0 and S_1, respectively). The difference between the frequencies in this mode is qualitatively compatible with the experimentally observed spacing of 100–130 cm^{-1} of the shoulders superimposed on the first major feature in the spectrum. While the nitro pyramidalization mode may be considered for this assignment as well, the calculated

frequencies are 801 cm^{-1} and 547 cm^{-1} in S_0 and S_1, respectively, and the energy difference therefore does not match the observed pattern.

In addition to spectral congestion, ultrafast experiments by Michenfelder *et al*.[18] show that the excited state lifetime of *p*-NP is very short (0.3 ps), leading to substantial lifetime broadening (ca. 18 cm^{-1}). The same experiments also suggest that triplet states, which are close in energy in the case of *p*- and *o*-NP (see Fig. S7 in ESI) do not offer efficient relaxation pathways for NPs, and we therefore assume that they are not relevant for the observed broadening. The authors invoked a conical intersection coupling S_1 and S_0 along the nitro torsion mode as the mechanism for ultrafast relaxation. While neither their calculations nor our own corroborate the existence of such a conical intersection, both sets of computations should only be taken as qualitative.

The spacing between the two main features of the spectrum is 730 cm^{-1}, similar in magnitude to the spacing between the regions of high intensity in the spectrum of *m*-NP. At the same time, there are similar calculated contractions of the C-N bond and extensions of the N-O bonds upon excitation. The calculated vertical excitation energy for the S_2 state is 2200 cm^{-1} above that of the S_1 state and carries zero oscillator strength. Based on these arguments, we suspect that the two peaks are regions in the spectrum with a difference of one quantum of characteristic Franck-Condon active modes, similar to those in *m*-NP. We note, however, that while this assignment is plausible, it is by no means assured. Unfortunately, Franck-Condon simulations this high above the band origin will be unreliable because of the anharmonicity in the nitro torsion and nitro pyramidalization, making a quantitative comparison with calculations problematic. Similarly, the very large difference between calculated vertical excitation energy and the band origin, combined with the multi-reference nature of the molecule introduces sufficient uncertainty into the computational results to offer only a tentative assignment.

Ortho-Nitrophenolate

Similar to *p*-NP, the spectrum of *o*-NP is broad, even at the cryogenic temperatures used in the present work (see Fig. 2). The spectrum has a smooth onset at ca. 20500 cm^{-1}, and shows irregularly spaced peaks at 21930 cm^{-1}, 23000 cm^{-1}, 23600 cm^{-1}, and 24200 cm^{-1}. The peak at 23000 cm^{-1} is the apparent vertical excitation energy. There is no regular substructure that could be associated with vibrational features. Low parent ion signal together with low laser pulse energies prevented us from acquiring data at higher wavenumbers. Similar to *p*-NP, excitation of *o*-NP to the S_1 state is not dominated by charge transfer, but rather has significant π-π^* character (change in the dipole moment 1.6 Debye, see Fig. 3 for difference densities and partial charges and Fig. S3 for frontier orbitals).

Results from excited state calculations show that there are two close-lying states in the Franck-Condon region with a separation of only 167 cm^{-1} (see Fig. 8). Optimization of the geometries of these excited states show that the S_1 state (oscillator strength 0.2033) has a twisted nitro group (perpendicular to the aromatic ring), and that the nitro group is pyramidalized, similar to the S_1 state in *p*-NP (see Fig. 5). The S_1 band origin is 17604 cm^{-1} above the ground state. The S_2 state (oscillator strength 10^{-4}) has its band origin at 21700 cm^{-1}, and has planar geometry. In the Franck-Condon region, the sequence of the two states is reversed, i.e., the S_2 state (vertical excitation energy 26963 cm^{-1}) is below the S_1 state (vertical excitation energy 27130 cm^{-1}). The close proximity of the two states in the Franck-Condon region suggests that the two electronic states may strongly mix (at the very least mediated by vibrations), invalidating the oscillator strength estimates obtained from our simple TD-DFT calculations. The close proximity and the reversal of their sequence in the Franck-Condon region also strongly suggest that these two states

have a conical intersection, even if our calculations must be viewed with caution, given the multi-reference nature of the ion. Excitation in the low-frequency modes such as the torsion and pyramidalization vibrations may lead the molecule to explore these coordinates in the S_1 state. The measured lifetime of the excited state in *o*-NP is 0.3 ps,[18] similar to *p*-NP. While one may expect the S_2 state to show well-structured vibrational features, the S_1 state should have a congested spectrum, similar to the case of *p*-NP. Along these lines, lifetime effects, spectral congestion and S_1/S_2 mixing make the observed absence of resolved vibrational features not surprising, and preclude a deeper analysis of the experimental spectrum.

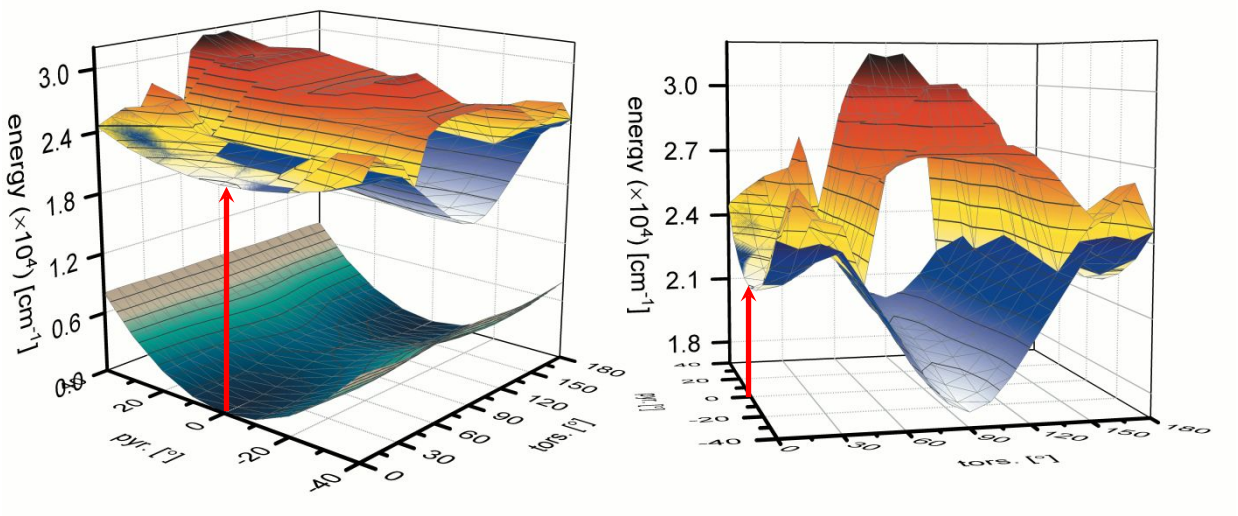

Fig. 8 Potential energy surfaces of the ground and first two excited states of *o*-NP (left) and a zoomed-in view of the first and second excited states (right). The ground state (S_0) is shown with a blue-to-gray color scheme. The first excited state (S_1) is shown in a white-to-blue color scheme and the second excited state (S_2) is shown in a yellow-to-red color scheme. These plots are shown as a function of nitro torsion (tors.) and pyramidalization (pyr.) angles, with energies given relative to the ground state (S_0). The point on the graph indicated by the red arrow shows the point of vertical excitation from the relaxed ground state geometry.

Summary

Despite the chemical similarity of the three isomers of NP, their spectra and excited state dynamics are very different. While a zero-order picture based on charge distribution arguments qualitatively captures the similarity of the excitation energies in *o*- and *p*-NP, and their contrast to *m*-NP, the photophysics of the three isomers offers a rich variety of different effects, much more complex than one would expect for such a set of simple systems. In particular, the associated broadening mechanisms are different for all three systems. In *m*-NP, the only broadening effects active in the electronic band origin region of the S_1 state seem to be lifetime and rotational contours, allowing the observation of well-resolved vibrational peaks. In contrast, both *p*- and *o*-NP spectra are broad. The *para* isomer suffers from spectral congestion due to a large geometry difference between S_0 and S_1 states, in addition to a much shorter excited state lifetime than *m*-NP. In *o*-NP, the close proximity of the second excited electronic state leads to additional broadening, and makes any deeper interpretation of the observed spectrum impossible. Cryogenic ion spectroscopy allows a much more detailed look into the excited state structure and the differences of the three NP isomers than would be possible at room temperature or in solution, particularly for *m*- and *p*-NP.

Acknowledgements

We gratefully acknowledge the National Science Foundation for support of this work under Grant CHE-1361814. This research was performed while L.G.D. held an NRC Research Associateship award at NIST. This work utilized the RMACC Summit supercomputer, which is supported by the National Science Foundation (awards ACI-1532235 and ACI-1532236), the University of Colorado Boulder, and Colorado State University. The Summit supercomputer is a joint effort of

the University of Colorado Boulder and Colorado State University. We thank Dr. Andrew Kortyna for help with PGOPHER, and P. Bryan Changala for helpful discussion on the calculation of the potential energy surfaces.

References

1. Z. R. Grabowski, K. Rotkiewicz and W. Rettig, *Chem. Rev.*, 2003, **103**, 3899-4032.
2. D. L. Ashford, M. K. Gish, A. K. Vannucci, M. K. Brennaman, J. L. Templeton, J. M. Papanikolas and T. J. Meyer, *Chem. Rev.*, 2015, **115**, 13006-13049.
3. H.-C. Lin and B.-Y. Jin, *Materials*, 2010, **3**, 4214.
4. N. Monahan and X. Y. Zhu, *Annu. Rev. Phys. Chem.*, 2015, **66**, 601-618.
5. L. R. Dalton, P. Günter, M. Jazbinsek, O.-P. Kwon and P. A. Sullivan, *Organic Electro-Optics and Photonics: Molecules, Polymers, and Crystals*, Materials Research Society and Cambridge University Press, Cambridge, United Kingdom, 2015.
6. J.-L. Brédas, D. Beljonne, V. Coropceanu and J. Cornil, *Chem. Rev.*, 2004, **104**, 4971-5004.
7. M. Zimmer, *Chem. Rev.*, 2002, **102**, 759-782.
8. F. Bureš, *RSC Adv.*, 2014, **4**, 58826-58851.
9. M.-B. S. Kirketerp, M. Å. Petersen, M. Wanko, L. A. E. Leal, H. Zettergren, F. M. Raymo, A. Rubio, M. Brøndsted Nielsen and S. Brøndsted Nielsen, *ChemPhysChem*, 2009, **10**, 1207-1209.
10. M. B. S. Kirketerp, M. Å. Petersen, M. Wanko, H. Zettergren, A. Rubio, M. Brøndsted Nielsen and S. Brøndsted Nielsen, *ChemPhysChem*, 2010, **11**, 2495-2498.
11. M. Wanko, J. Houmoller, K. Stochkel, M.-B. S. Kirketerp, M. Å. Petersen, M. Brøndsted Nielsen, S. Brøndsted Nielsen and A. Rubio, *Phys. Chem. Chem. Phys.*, 2012, **14**, 12905-12911.

12. J. Houmøller, M. Wanko, K. Støchkel, A. Rubio and S. Brøndsted Nielsen, *J. Am. Chem. Soc.*, 2013, **135**, 6818-6821.

13. S. Brøndsted Nielsen, M. Brøndsted Nielsen and A. Rubio, *Acc. Chem. Res.*, 2014, **47**, 1417-1425.

14. J. Houmøller, M. Wanko, A. Rubio and S. Brøndsted Nielsen, *J. Phys. Chem. A*, 2015, **119**, 11498-11503.

15. M. H. Stockett, M. Boesen, J. Houmøller and S. Brøndsted Nielsen, *Angew. Chem.*, 2017, **129**, 3544-3549.

16. J. Kozłowska, M. Wielgus and W. Bartkowiak, *Comput. Theor. Chem.*, 2013, **1014**, 49-55.

17. S. K. Panja, N. Dwivedi and S. Saha, *RSC Adv.*, 2016, **6**, 105786-105794.

18. N. C. Michenfelder, H. A. Ernst, C. Schweigert, M. Olzmann and A. N. Unterreiner, *Phys. Chem. Chem. Phys.*, 2018, **20**, 10713-10720.

19. S. Xu, S. Gozem, A. I. Krylov, C. R. Christopher and J. M. Weber, *Phys. Chem. Chem. Phys.*, 2015, **17**, 31938-31946.

20. T. Yanai, D. P. Tew and N. C. Handy, *Chem. Phys. Lett.*, 2004, **393**, 51-57.

21. A. Dreuw, J. L. Weisman and M. Head-Gordon, *J. Chem. Phys.*, 2003, **119**, 2943-2946.

22. A. Dreuw and M. Head-Gordon, *J. Am. Chem. Soc.*, 2004, **126**, 4007-4016.

23. E. D. Glendening, A. E. Reed, J. E. Carpenter and F. Weinhold, *QCPE Bull.*, 1990, **10**, 58.

24. M. J. Frisch, G. W. Trucks, H. B. Schlegel, G. E. Scuseria, M. A. Robb, J. R. Cheeseman, G. Scalmani, V. Barone, G. A. Petersson, H. Nakatsuji, et al. *Gaussian 16 Rev. B.01*, Wallingford, CT, 2016.

25. J. Mikosch, H. Kreckel, R. Wester, R. Plašil, J. Glosík, D. Gerlich, D. Schwalm and A. Wolf, *J. Chem. Phys.*, 2004, **121**, 11030-11037.

26. O. Asvany and S. Schlemmer, *Int. J. Mass Spectrom.*, 2009, **279**, 147-155.

27. R. Wester, *J. Phys. B: At. Mol. Opt. Phys.*, 2009, **42**, 154001.

28. S. Xu, J. E. T. Smith and J. M. Weber, *J. Chem. Phys.*, 2016, **145**, 024304.

29. C. M. Western, *J. Quant. Spectrosc. Radiat. Transfer*, 2017, **186**, 221-242.